


Abnormal specific heat enhancement and non-Fermi-liquid behavior in the heavy-fermion system $U_2Cu_{17-x}Ga_x$ ($5 \leq x \leq 8$)

E. Svanidze, A. Amon, Yu. Prots, A. Leithe-Jasper, and Yu. Grin

Max-Planck-Institut für Chemische Physik fester Stoffe, Nöthnitzer Straße 40, Dresden 01187, Germany
 (Received 31 December 2017; published 26 March 2018)

In the antiferromagnetic heavy-fermion compound U_2Zn_{17} , the Sommerfeld coefficient γ can be enhanced if all Zn atoms are replaced by a combination of Cu and Al or Cu and Ga. In the former ternary phase, glassy behavior was observed, while for the latter, conflicting ground-state reports suggest material quality issues. In this work, we investigate the $U_2Cu_{17-x}Ga_x$ substitutional series for $4.5 \leq x \leq 9.5$. In the homogeneity range of the phase with the Th_2Zn_{17} -type of crystal structure, all samples exhibit glassy behavior with $0.6 \text{ K} \leq T_f \leq 1.8 \text{ K}$. The value of the electronic specific heat coefficient γ in this system exceeds $900 \text{ mJ/mol}_U \text{ K}^2$. Such a drastic effective-mass enhancement can possibly be attributed to the effects of structural disorder, since the role of electron concentration and lattice compression is likely minimal. Crystallographic disorder is also responsible for the emergence of non-Fermi-liquid behavior in these spin-glass materials, as evidenced by logarithmic divergence of magnetic susceptibility, specific heat, and electrical resistivity.

DOI: [10.1103/PhysRevB.97.115148](https://doi.org/10.1103/PhysRevB.97.115148)

I. INTRODUCTION

Uranium intermetallic compounds exhibit a wide range of exotic properties: unconventional superconductivity and quantum criticality, complex magnetic configurations, as well as heavy-fermion and non-Fermi-liquid behaviors [1–11]. The coexistence of the latter two phenomena has been observed in a number of materials, and while it has been noted that the role of interaction between the local moments and conduction electrons plays an important role, complete understanding of the underlying mechanisms is still lacking. The majority of uranium-based systems have a low concentration of $5f$ atoms [2,3], which makes it possible to invoke the single-ion Kondo description [6,12,13]. A multichannel Kondo scenario [14,15] and proximity to a quantum critical point [16,17] have been suggested as possible mechanisms for the breakdown of the Fermi-liquid theory. However, experimentally, many systems have been shown to exhibit a spin-glass state preempting the onset of non-Fermi-liquid behavior: Pd-substituted UCu_5 [18–20], Y-substituted UAl_2 [21], Y- [22–27] and Sc/B-substituted [28,29] UPd_3 , Y- and La-substituted UPd_2Al_3 [30–32], as well as stoichiometric URh_2Ge_2 [33,34]. This is more readily understood within the disorder models, which suggest that the Griffiths phase appears in these materials as a consequence of Kondo disorder [19,35–42]. Careful analysis of novel heavy-fermion compounds will help investigate the validity of proposed theories and, perhaps, provide a unifying model for the breakdown of Fermi-liquid theory in all classes of heavy-fermion materials.

As mentioned above, compounds with low concentration, and, therefore, high coordination of uranium atoms, provide one avenue in the search for new heavy-fermion materials. This approach has proved effective in the case of antiferromagnetic U_2Zn_{17} [43] and UCd_{11} [44], as well as superconducting UBe_{13} [45]. Considering the fact that these systems exhibit the highest values of the Sommerfeld coefficient γ among all U-

based heavy fermions, several attempts to further enhance the electronic specific heat coefficient were performed. Pressure experiments revealed that even though antiferromagnetic order is suppressed, γ remains unaffected [46]. Given a large number of R_2Zn_{17} ($R = \text{La-Nd, Sm-Lu, Th, U, Pu}$) compounds, several substitutions on the U site were previously reported [47–49]. Partial substitution of U with Th suppressed antiferromagnetic order in U_2Zn_{17} [47], while replacement with La resulted in an emergence of the Kondo effect [48,49]. It was also noticed that substitution on the Zn site, e.g., by Cu, is much more effective in suppressing antiferromagnetism [47] in comparison with substitution on the U site. Given that the combination of Cu and Ga electronically mimics Zn, a ternary phase with the Th_2Zn_{17} type of the crystal structure (Fig. 1) should be considered.

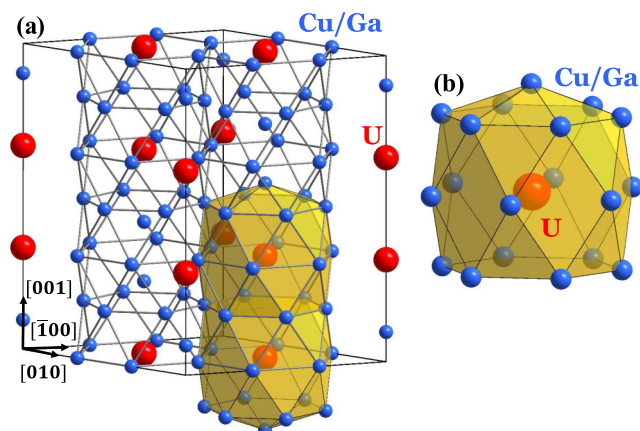


FIG. 1. Crystal structure of $U_2Cu_{17-x}Ga_x$ (space group $R\bar{3}m$, structure type Th_2Zn_{17}): (a) U atoms (large red spheres) are located within hexagonal channels along [001], formed by Cu/Ga atoms (small blue spheres). (b) Coordination of U atoms by 19 Cu/Ga atoms.

Indeed, it was previously noted that a complete replacement of Zn atoms is possible with a combination of Cu and Ga [50–52] or Cu and Al [51,53–56]. Resultant materials exist in only a limited composition range, with the lattice compression between 6% and 9%, depending on the ratio of Cu to Ga or Al. In the $U_2Cu_{17-x}Al_x$ ($5 \leq x \leq 10$) phase [55], dissimilarity of atomic radii of Cu ($r_{Cu} = 1.28 \text{ \AA}$) and Al ($r_{Al} = 1.43 \text{ \AA}$) atoms gives rise to disorder effects. This disorder, along with geometric frustration of U atoms, resulted in a spin-glass behavior for several compositions [55]. For the $U_2Cu_{17-x}Ga_x$ system, disorder effects are expected to be diminished, given the similarity of atomic radii of Cu ($r_{Cu} = 1.28 \text{ \AA}$) and Ga ($r_{Ga} = 1.37 \text{ \AA}$). However, one report indicates glassy behavior [55], while another claims paramagnetism down to $T = 1.1 \text{ K}$ [52].

In this work, we investigate the substitutional series $U_2Cu_{17-x}Ga_x$ with $4.5 \leq x \leq 9.5$. Single-phase samples are obtainable only for $5.5 \leq x \leq 7.5$. All of the materials exhibit values of the Sommerfeld coefficient γ exceeding $900 \text{ mJ/mol}_U \text{ K}^2$. A glassy transition, with freezing temperature $0.6 \text{ K} \leq T_f \leq 1.8 \text{ K}$, is observed for all x . Additionally, non-Fermi-liquid behavior is evident from magnetic susceptibility, specific heat, and resistivity data. It is likely that both the dramatic effective-mass enhancement and the breakdown of the Fermi-liquid theory are brought on by the effects of crystallographic disorder, which results from mixing of Cu and Ga at the four crystallographic sites, as well as twinning.

II. EXPERIMENTAL METHODS

Polycrystalline samples of $U_2Cu_{17-x}Ga_x$ ($4.5 \leq x \leq 9.5$) were synthesized by arc melting U (sheet, Goodfellow, 99.98%), Cu (granules, Chempur, 99.95%), and Ga (pellets, Chempur, 99.9999%) in stoichiometric ratios. Given mass losses during the preparation of no more than 0.5%, nominal compositions are used throughout the text. The as-cast buttons were annealed for a week at $750 \text{ }^\circ\text{C}$ in an argon atmosphere and then cooled slowly to room temperature. All sample handling was performed in an argon-filled glove box [$p(O_2/H_2O) < 0.1 \text{ ppm}$], dedicated to the handling of U-containing samples [57]. Small amounts of nitrogen are typically present in the glove-box system, which lead to the formation of UN. It was, however, noticed that both as-cast and annealed samples did not exhibit any marked air or moisture sensitivity.

Powder x-ray diffraction on the annealed samples was performed on a HUBER G670 imaging plate Guinier camera ($CuK\alpha_1$ radiation $\lambda = 1.54056 \text{ \AA}$). Phase identification was done using the WINXPOW software [58]. Single-crystal diffraction data were collected for the single crystals with $x = 6.5, 7, \text{ and } 7.5$ on a Rigaku AFC7 diffractometer equipped with a Saturn 724+ CCD detector, using $MoK\alpha$ radiation ($\lambda = 0.71073 \text{ \AA}$). All crystallographic calculations (data evaluation, crystal structure refinements, etc.) were performed with the WINCSD software [59]. The crystallographic information for the investigated single crystals is presented in Tables I–III.

TABLE I. Crystallographic data of $U_2Cu_{17-x}Ga_x$ ($x = 6.5$).

Crystal system, space group		Trigonal, $R\bar{3}m$ (No. 166)				
Formula units per unit cell		$Z = 3$				
Composition		$U_2Cu_{10.5}Ga_{6.5}$				
$2\theta_{max}$		80°				
$N(hkl)_{measured}$		5437				
$N(hkl)_{unique}$		791				
$N(hkl)_{observed} [F_{hkl} > 4\sigma(F)]$		630				
R_{int}/R_σ		0.054/0.060				
Refined parameters		23				
R_F/wR_F^2 ^a		0.073/0.079				
Residual electron density maximum		11.4/−6.0				
Twin fraction refined		0.85/0.15				
Atom	Site	x/a	y/b	z/c	B_{eq} ^b	Occ. ^c
U1	6c	0	0	0.34113(9)	1.16(2)	1
Cu/Ga1	9d	1/3	1/6	1/6	0.91(7)	0.61/0.39
Cu/Ga2	18h	0.3292(3)	$x/2$	0.5154(2)	0.85(5)	0.61/0.39
Cu/Ga3	18f	0.2951(2)	0	0	0.73(6)	0.61/0.39
Cu/Ga4	6c	0	0	0.1025(3)	0.73(6)	0.61/0.39

$$^a w_i = \ln(F_{obs}^4)^{-1}.$$

$$^b B_{eq} = 1/3[B_{11}a^{*2}a^2 + \dots + 2B_{23}b^*c^*bc \cos(\alpha)].$$

^cCu/Ga ratio was fixed according to the nominal composition of the sample.

Chemical composition of polished samples was studied using energy-dispersive x-ray spectroscopy with a Jeol JSM 6610 scanning electron microscope equipped with an UltraDry EDS detector (ThermoFisher NSS7). The semiquantitative analysis was performed with a 25 keV acceleration voltage and an $\approx 3 \text{ nA}$ beam current. Quantitatively, the areas corresponding to different phases were estimated using the OLYMPUS STREAM software.

TABLE II. Crystallographic data of $U_2Cu_{17-x}Ga_x$ ($x = 7$).

Crystal system, space group		Trigonal, $R\bar{3}m$ (No. 166)				
Formula units per unit cell		$Z = 3$				
Composition		$U_2Cu_{10}Ga_7$				
$2\theta_{max}$		80°				
$N(hkl)_{measured}$		6044				
$N(hkl)_{unique}$		791				
$N(hkl)_{observed} [F_{hkl} > 4\sigma(F)]$		627				
R_{int}/R_σ		0.049/0.025				
Refined parameters		23				
R_F/wR_F^2 ^a		0.047/0.053				
Residual electron density maximum		0.38/−0.28				
Twin fraction refined		0.66/0.34				
Atom	Site	x/a	y/b	z/c	B_{eq} ^b	Occ. ^c
U1	6c	0	0	0.34089(6)	1.02(1)	1
Cu/Ga1	9d	1/3	1/6	1/6	0.79(4)	0.59/0.41
Cu/Ga2	18h	0.3291(3)	$x/2$	0.5150(1)	0.77(3)	0.59/0.41
Cu/Ga3	18f	0.2948(2)	0	0	0.77(3)	0.59/0.41
Cu/Ga4	6c	0	0	0.1027(2)	0.72(4)	0.59/0.41

$$^a w_i = \ln(F_{obs}^4)^{-1}.$$

$$^b B_{eq} = 1/3[B_{11}a^{*2}a^2 + \dots + 2B_{23}b^*c^*bccos(\alpha)].$$

^cCu/Ga ratio was fixed according to the nominal composition of the sample.

TABLE III. Crystallographic data of $U_2Cu_{17-x}Ga_x$ ($x = 7.5$).

Parameter	Value					
Crystal system, space group	Trigonal, $R\bar{3}m$ (No. 166)					
Formula units per unit cell	$Z = 3$					
Composition	$U_2Cu_{9.5}Ga_{7.5}$					
$2\theta_{\max}$	80°					
$N(hkl)_{\text{measured}}$	5641					
$N(hkl)_{\text{unique}}$	791					
$N(hkl)_{\text{observed}} [F_{hkl} > 4\sigma(F)]$	647					
R_{int}/R_σ	0.037/0.036					
Refined parameters	23					
R_F/wR_F^{2a}	0.056/0.062					
Residual electron density maximum	5.5/−3.6					
Twin fraction refined	0.91/0.09					
Atom	Site	x/a	y/b	z/c	B_{eq}^b	Occ. ^c
U1	6c	0	0	0.34064(6)	0.98(3)	1
Cu/Ga1	9d	1/3	1/6	1/6	0.91(5)	0.56/0.44
Cu/Ga2	18h	0.3285(2)	$x/2$	0.5151(1)	0.90(3)	0.56/0.44
Cu/Ga3	18f	0.2949(2)	0	0	0.95(3)	0.56/0.44
Cu/Ga4	6c	0	0	0.1031(2)	0.79(4)	0.56/0.44

$$^a w_i = \ln(F_{\text{obs}}^4)^{-1}.$$

$$^b B_{\text{eq}} = 1/3[B_{11}a^{*2}a^2 + \dots + 2B_{23}b^*c^*bccos(\alpha)].$$

^cCu/Ga ratio was fixed according to the nominal composition of the sample.

All thermodynamic and transport measurements were performed on the annealed specimens in the $5.5 \leq x \leq 7.5$ composition range, marked by colored symbols in Figs. 2(a) and 2(b). Temperature- and field-dependent dc magnetization measurements were carried out in a Quantum Design (QD) magnetic property measurement system for temperatures between 2 and 300 K and for applied magnetic fields up to $H = 7$ T. Heat capacity was measured from 0.4 to 10 K in magnetic fields up to $H = 9$ T using a QD physical property measurement system (PPMS). The dc resistivity measurements in a temperature range from 0.4 K to 300 K were carried out using the standard four-probe method in the QD PPMS in $H = 0$ and $H = 9$ T. Platinum wires were attached to the polished surfaces of a bar-shaped polycrystalline sample using spot welding.

III. RESULTS AND DISCUSSION

The crystal structure of $U_2Cu_{17-x}Ga_x$ [Fig. 1(a)] can be derived from the binary compound U_2Zn_{17} , which was reported to form in the rhombohedral Th_2Zn_{17} structure type (space group $R\bar{3}m$) [50,51,60]. Zinc can be replaced by a mixture of Cu and Ga in the narrow composition range with $5 \leq x \leq 8$, as marked by the gray region in Figs. 2(a) and 2(b). Uranium atoms (red) occupy the 6c position and are surrounded by 19 Zn atoms (here Cu/Ga, blue) located in the 6c, 9d, 18f, and 18h crystallographic positions. The Cu/Ga sublattice forms hexagonal channels along [001], which contain the U atoms [Fig. 1(a)]. Similar hexagonal channels are also found

in the $CaCu_5$ structure type. In the Th_2Zn_{17} structure type, every third Th atom in the $CaCu_5$ -like channel is replaced by a pair of Zn atoms or, in the case of $U_2Cu_{17-x}Ga_x$, Cu and/or Ga atoms. The crystal structure was solved and refined from single-crystal diffraction data recorded on crystals of the compositions $x = 6.5, 7$, and 7.5 (Tables I–III, respectively). Careful examination of the single-crystal diffraction data in reciprocal space showed that the observed Laue class appears to be higher than trigonal. This is indicative of the typical obverse-reverse twinning tendency of rhombohedral structures [61]. The twin law was described by the matrix $(-1 \ 0 \ 0 \ 0 \ -1 \ 0 \ 0 \ 0 \ 1)$. The obtained structure models confirm the Th_2Zn_{17} structure type for all investigated compositions, where the refined atomic coordinates showed only minute differences between the three compositions. Uranium atoms in $U_2Cu_{17-x}Ga_x$ have a high coordination number of 19 [Fig. 1(b)], with Cu/Ga atoms at distances $3.11 \text{ \AA} \leq d_{U-Cu/Ga} \leq 3.45 \text{ \AA}$ and one U atom at a larger distance $d_{U-U} = 4.32 \text{ \AA}$. The similar scattering strengths of Cu and Ga make it impossible to distinguish between the two elements and determine whether Cu and Ga are occupying the Zn sublattice of the Th_2Zn_{17} structure type in a statistical distribution or whether ordering of Cu and Ga takes place [62]. This issue was reported previously for both $U_2Cu_{17-x}Ga_x$ and $U_2Cu_{17-x}Al_x$ systems [51]. We have attempted to address this by examining the single-crystal diffraction data and performing NMR analysis, but neither approach was able to resolve possible Cu and Ga ordering. Therefore, the occupancies of the (Cu, Ga) positions were fixed in the ratio corresponding to the sample composition.

Previously reported crystallographic data of the $U_2Cu_{17-x}Ga_x$ phase are conflicting as one report claims a lattice expansion of about 2% [51], while another notes that the lattice parameters are virtually independent of x [52]. The behavior of lattice parameters a and c , along with the unit cell volume V as a function of x , obtained from the powder x-ray diffraction data for $U_2Cu_{17-x}Ga_x$ ($4.5 \leq x \leq 9.5$) is shown in Figs. 2(a) and 2(b). Lattice parameters for the $5.5 \leq x \leq 7.5$ samples are given in Table IV: both a and c increase continuously with x , expanding the volume by about 3.5%. The c/a ratio remains nearly constant over the whole composition range of the phase. The lattice parameters show negative (a) and positive (c) deviations from Vegard's law ($r_{Ga} = 1.37 \text{ \AA}$, $r_{Cu} = 1.28 \text{ \AA}$).

The multiphase nature of the samples outside of the $5.5 \leq x \leq 7.5$ composition range was confirmed by both x-ray powder diffraction and energy-dispersive x-ray spectroscopy. The phases in equilibrium with the $U_2Cu_{17-x}Ga_x$ phase include $UCu_{3+x}Ga_{2-x}$ (antiferromagnet with $T_N = 5\text{--}15$ K [63], $\gamma = 200\text{--}350$ mJ/mol_U K² [63], space group $P6/mmm$ [51]), UGa_3 (antiferromagnet with $T_N = 66$ K [64], $\gamma = 50$ mJ/mol_U K² [65], space group $Pm\bar{3}m$ [66]), and $U_{14}Cu_{44+x}Ga_{7-x}$ (antiferromagnet with $T_N = 16$ K [67], $\gamma = 200$ mJ/mol_U K² [67], space group $P6/m$ [51]). The presence of minority phases can, perhaps, explain conflicting reports of the ground state in the $U_2Cu_{17-x}Ga_x$ system [52,55].

For the $5.5 \leq x \leq 7.5$ samples, the only impurities present are UN and Cu_9Ga_4 , in a total amount of less than 3%. These samples are marked by colored symbols in Figs. 2(a) and 2(b), with the respective colors kept consistent throughout the

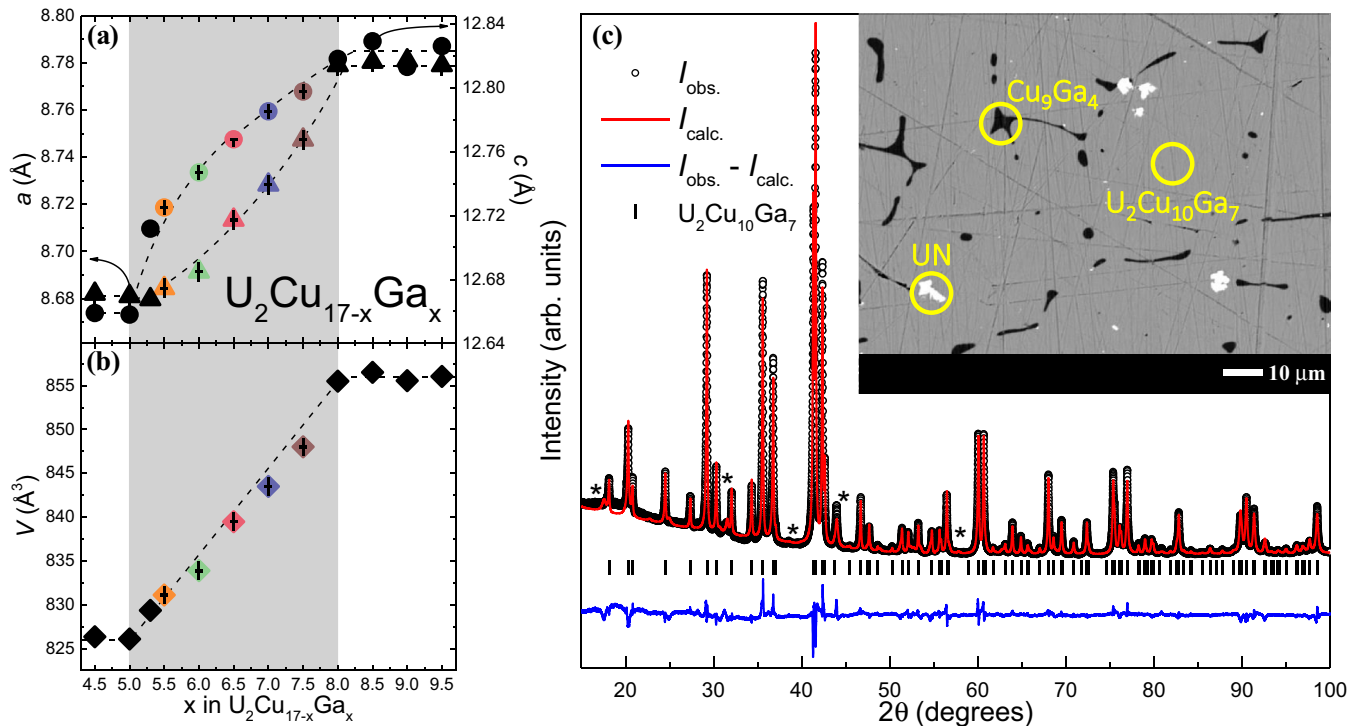


FIG. 2. Crystallographic data and microstructure of $U_2Cu_{17-x}Ga_x$ for $4.5 \leq x \leq 9.5$: (a) Evolution of lattice parameters a (left axis, triangles) and c (right axis, circles). (b) Unit cell volume V as a function of x . The gray region marks the homogeneity range of the $U_2Cu_{17-x}Ga_x$ phase. Colored symbols represent x values investigated in this work, while black symbols indicate multiphase samples. (c) Powder diffraction pattern for the $x = 7$ sample: I_{obs} is represented by black circles, while I_{calc} and $I_{obs} - I_{calc}$ are shown as a red and blue lines, respectively. The black tick marks represent peak positions for the Th_2Zn_{17} structure type. Reflections of the minority phases UN and Cu_9Ga_4 are marked by asterisks. Inset: the backscatter electron micrograph of an annealed polycrystalline sample shows, besides the main phase (gray), the impurity phases UN (white) and Cu_9Ga_4 (black), which amount to less than 3%.

rest of the paper. An example of a powder x-ray diffraction pattern and a backscatter electron micrograph of the $x = 7$ sample is shown in Fig. 2(c). The reflections of minority phases UN and Cu_9Ga_4 are marked by asterisks on the diffraction pattern. They can be seen as white (UN) and black (Cu_9Ga_4) regions in the microstructure pattern. These phases do not affect the conclusions of this paper since Cu_9Ga_4 exhibits a temperature-independent magnetic susceptibility, while UN orders antiferromagnetically below $T_N = 51$ K with a Sommerfeld coefficient $33 \text{ mJ/mol}_U \text{ K}^2 \leq \gamma \leq 49 \text{ mJ/mol}_U \text{ K}^2$ [68,69].

Temperature- and field-dependent magnetization of $U_2Cu_{17-x}Ga_x$ ($5.5 \leq x \leq 7.5$) is shown in Fig. 3. Curie-Weiss behavior is observed for all compositions, as evidenced by the inverse magnetic susceptibility, shown in Fig. 3(a) (M_0 is the temperature-independent contribution to the magnetic susceptibility). As can be seen from the inset of Fig. 3(a), no ordering is observed down to $T = 2$ K. However, we believe a glassy transition takes place at lower temperatures, $0.6 \text{ K} \leq T_f \leq 1.8 \text{ K}$, as evidenced by the specific heat data presented below. Magnetic correlations are, indeed, expected to occur in this material, given that the U-U distance in $U_2Cu_{17-x}Ga_x$ ($d_{U-U} = 4.24\text{--}4.27 \text{ \AA}$) is close to that of U_2Zn_{17} ($d_{U-U} = 4.39 \text{ \AA}$) [43] and is above the Hill limit ($d_{U-U} = 3.4\text{--}3.6 \text{ \AA}$) [70].

Glassy ground states arise in systems for which both frustration and disorder are present. Geometric frustration is more readily realized on a triangular or Kagome lattice, with the majority of glassy systems exhibiting antiferromagnetic coupling [71,72]. Most uranium-based materials order antiferromagnetically [2,3], suggesting that one condition for glassiness is already fulfilled. Disorder, on the other hand, can be brought on by chemical substitution. Among glassy materials, two regimes are possible: spin- and cluster-glasses. Cluster-glass materials are glassy systems in which the spins exhibit short-range correlations within a cluster, while the clusters themselves show the cooperative freezing characteristic of spin-glasses [71,72]. A majority of uranium-based systems are classified as spin-glasses, which can perhaps be explained by the very low concentration of U atoms. Consequently, for the case of $U_2Cu_{17-x}Ga_x$, the overlap of zero-field-cooled and field-cooled susceptibility data [inset of Fig. 3(a)] indicate that these transitions are likely spin-glass, rather than cluster-glass. For cluster-glass materials the irreversibility temperature T_{irr} is typically higher than the freezing temperature T_f [71,72], and, given the values of the freezing temperature T_f extracted from the specific heat data [Fig. 4(d) and Table IV], one would expect to see bifurcation of the zero-field-cooled and field-cooled data in the cluster-glass scenario. However, more concrete evidence for the cluster- vs spin-glass scheme can be achieved only via ac susceptibility analysis, which is

TABLE IV. Crystallographic data and physical properties of $U_2Cu_{17-x}Ga_x$ ($5.5 \leq x \leq 7.5$).

Quantity	Units	$x = 5.5$	$x = 6$	$x = 6.5$	$x = 7$	$x = 7.5$
a	Å	8.6844(8)	8.6914(8)	8.7134(1)	8.7283(9)	8.7474(6)
c	Å	12.7250(2)	12.7470(2)	12.7677(1)	12.7852(1)	12.7976(2)
$M/H(2K)$	emu/mol _U	0.049 ± 0.001	0.043 ± 0.001	0.045 ± 0.001	0.036 ± 0.001	0.040 ± 0.001
μ_{eff}	μ_B/U	2.74 ± 0.05	2.71 ± 0.05	2.74 ± 0.05	2.61 ± 0.05	2.38 ± 0.05
$M(T = 2 \text{ K}, H = 7 \text{ T})$	μ_B/U	0.41 ± 0.01	0.42 ± 0.01	0.44 ± 0.01	0.36 ± 0.01	0.40 ± 0.01
θ_W	K	-34 ± 5	-36 ± 5	-35 ± 5	-41 ± 5	-15 ± 5
T_f	K	0.6 ± 0.1	0.9 ± 0.1	1.3 ± 0.1	1.6 ± 0.1	1.8 ± 0.1
T_K	K	11.7 ± 0.1	11.4 ± 0.1	10.8 ± 0.1	7.5 ± 0.1	5.8 ± 0.1
$\gamma_1(H = 0)$	mJ/mol _U K ²	941 ± 10	941 ± 10	926 ± 10	956 ± 10	964 ± 10
$\gamma_1(H = 9 \text{ T})$	mJ/mol _U K ²	648 ± 10	664 ± 10	711 ± 10	767 ± 10	839 ± 10
$\gamma_2(H = 0)$	mJ/mol _U K ²	380 ± 10	383 ± 10	513 ± 10	467 ± 10	399 ± 10
$\gamma_2(H = 9 \text{ T})$	mJ/mol _U K ²	440 ± 10	459 ± 10	566 ± 10	531 ± 10	482 ± 10
$\gamma_3(H = 0)$	mJ/mol _U K ²	773 ± 10	888 ± 10	940 ± 10	967 ± 10	968 ± 10

rendered problematic due to the very low temperature of the transition.

As can be seen from Fig. 3(b), the low-temperature susceptibility follows $M/H \propto -\log_{10}T$ over roughly a decade in temperature, a clear signature of non-Fermi-liquid behavior [6]. This is reminiscent of what has been observed in other diluted uranium-based systems, for which non-Fermi-liquid behavior has been confirmed: Pd-substituted UCu_5 [73,74], Y- [73] and Np-substituted [75] UPd_3 , Y-substituted UAl_2 [21], and Th-substituted UPd_2Al_3 [12]. Magnetization parameters, extracted from temperature- and field-dependent susceptibility data, are summarized in Fig. 3(c) and in Table IV. The values of the magnetic susceptibility at the lowest temperature $M/H(2 \text{ K})$ are much higher than those of normal metals, signaling effective-mass enhancement. Comparable enhancement has been observed for $U_2Cu_{17-x}Al_x$ [55]; however, the values are generally higher for the case of $U_2Cu_{17-x}Ga_x$. This is consistent with higher values of the electronic specific heat coefficient γ , shown in Fig. 4(d). The magnitude of the effective magnetic moment μ_{eff} decreases as a function of x , with the maximum value of $2.74\mu_B/U$ for the $x = 5.5$ sample; this value is well below that expected for either $5f^3$ ($\mu_{\text{eff}} = 3.68\mu_B$) or $5f^2$ ($\mu_{\text{eff}} = 3.52\mu_B$) configurations, which can perhaps be explained by the itinerant nature of U atoms. In contrast, the value of the effective moment $\mu_{\text{eff}} = 3.6\mu_B/U$ for U_2Zn_{17} is consistent with the $5f^2$ configuration [43]. The values of the magnetic moment at lowest temperature and highest field $M(2 \text{ K}, 7 \text{ T})$, extracted from field-dependent magnetization data (not shown), are also lower than expected. The Weiss temperature θ_W is negative for all values of x , which is reminiscent of Kondo systems. Moreover, $|\theta_W| \gg T_f$ attests to the presence of frustration in $U_2Cu_{17-x}Ga_x$ ($5.5 \leq x \leq 7.5$).

Specific heat measurements of the $U_2Cu_{17-x}Ga_x$ ($5.5 \leq x \leq 7.5$) system are shown in Fig. 4. All of the $U_2Cu_{17-x}Ga_x$ materials can be classified as heavy-fermion materials, with $\gamma > 900 \text{ mJ/mol}_U \text{ K}^2$. A low-temperature plateau is observed for all compositions, as seen from Fig. 4(a), giving a value for the Sommerfeld coefficient $\gamma_1(H = 0)$. Such a feature in C_p/T is typically associated with freezing of the U magnetic moments, analogous to what has been observed in the case of Pd-substituted UCu_5 [18–20], Y-substituted UAl_2 [21],

La-substituted UPd_2Ga_3 [31,32], Y- [7,15,23,25,76] and Sc/B-substituted [28] UPd_3 . Logarithmic divergence of the specific heat $C/T \propto -\log_{10}T$ follows the plateau region, signaling non-Fermi-liquid behavior [8]. The freezing temperature T_f is estimated as the point at which the logarithmic divergence of the specific heat data is succeeded by constant C_p/T , with an example illustrated in Fig. 4(a) for the $x = 6.5$ sample. As can be seen from Fig. 4(d), $C_p/T(1.1 \text{ K}) = \gamma_3$ values are higher for $U_2Cu_{17-x}Ga_x$ (left axis, colored solid circles) compared to previous reports (left axis, black solid circles), as well as the $U_2Cu_{17-x}Al_x$ analogs (left axis, solid triangles). The values of γ_3 increase monotonically with x , which can be attributed to a monotonically increasing T_f . This agrees well with the trend of the $M/H(2 \text{ K})$ values described above. However, freezing temperatures T_f for the $U_2Cu_{17-x}Ga_x$ ($5.5 \leq x \leq 7.5$) series (right axis, open circles) are lower than those for the $U_2Cu_{17-x}Al_x$ analogs (right axis, open triangles). This can perhaps be explained by higher Weiss temperatures of the former [55], which in turn correspond to stronger U-U correlations. It is evident from Fig. 4(a) that the application of field (open symbols) suppresses the glassy state, diminishing the effective mass [$\gamma_1(H = 9 \text{ T})$].

Another way of estimating the value of the electronic specific heat coefficient $\gamma_2(H = 0)$ is to extrapolate the high-temperature data for which conventional Fermi-liquid behavior with phonon contribution $C_p/T \propto \gamma + \beta T^2$ is recovered, with fits shown in Fig. 4(b). In this case, application of magnetic field (open symbols) enhances the value of the Sommerfeld coefficient $\gamma_2(H = 9 \text{ T})$, as summarized in Fig. 4(c). Overall, the values of the electronic specific heat coefficient γ seem to be composition-independent. This signals that the dramatic mass enhancement is likely not caused by a change in electron concentration or lattice expansion, but rather crystallographic disorder effects. The effect of Cu/Ga mixing disorder likely arises from the atomic size difference, causing a local lattice strain. This strain is smaller for the $U_2Cu_{17-x}Ga_x$ series than for the $U_2Cu_{17-x}Al_x$ series, but bigger than that of U_2Zn_{17} . The influence of grain and/or twin boundaries on the physical properties should also be taken into consideration. As is evident from Fig. 5, twinning locally breaks translational symmetry, changing the environment of U atoms and their interaction

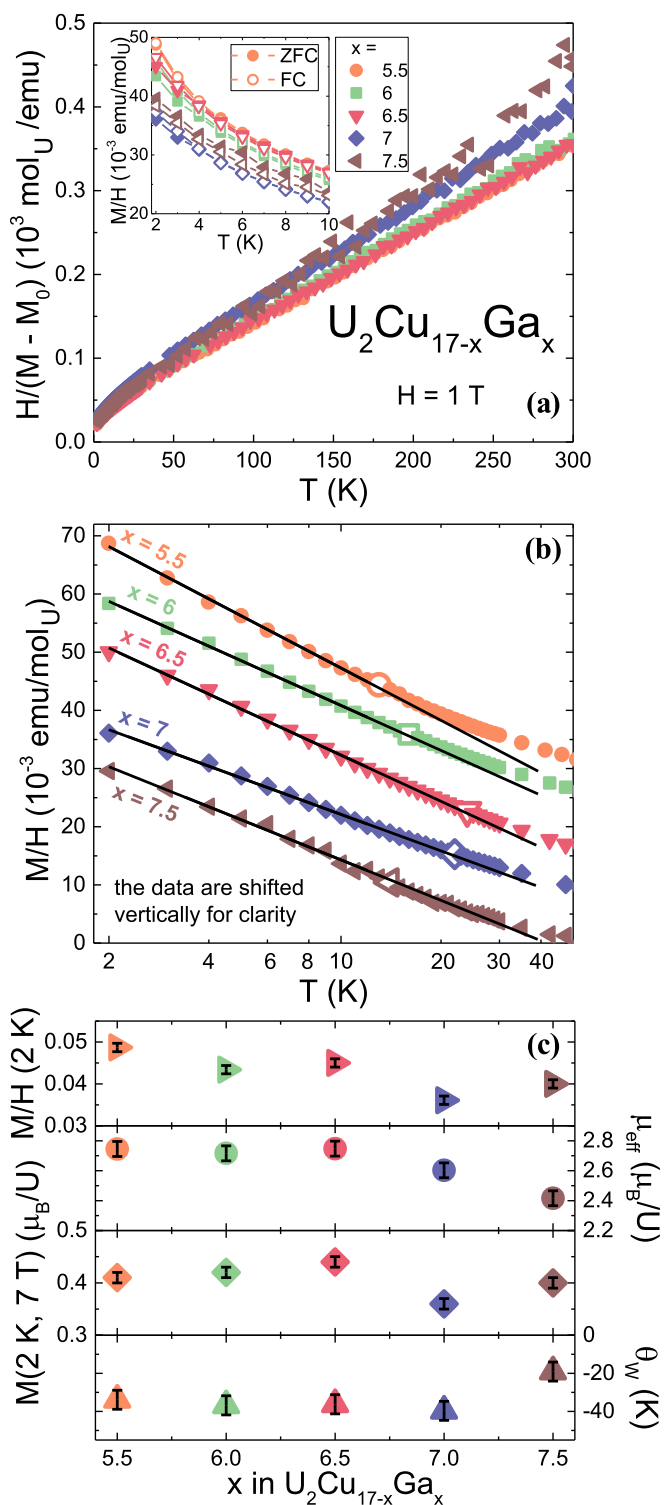


FIG. 3. Magnetic behavior of $U_2Cu_{17-x}Ga_x$ for $5.5 \leq x \leq 7.5$. (a) Temperature-dependent inverse magnetic susceptibility. Inset: zero-field-cooled (open symbols) and field-cooled (solid symbols) data are identical for all compositions. (b) Semilogarithmic plot of low-temperature susceptibility. The data are shifted vertically for clarity. (c) Summary of parameters extracted from temperature- and field-dependent magnetization data: magnetic susceptibility at the lowest temperature $M/H(T = 2 \text{ K})$, effective magnetic moment μ_{eff} , magnetic moment at the lowest temperature and highest field $M(2 \text{ K}, 7 \text{ T})$, and Weiss temperature θ_w as a function of x .

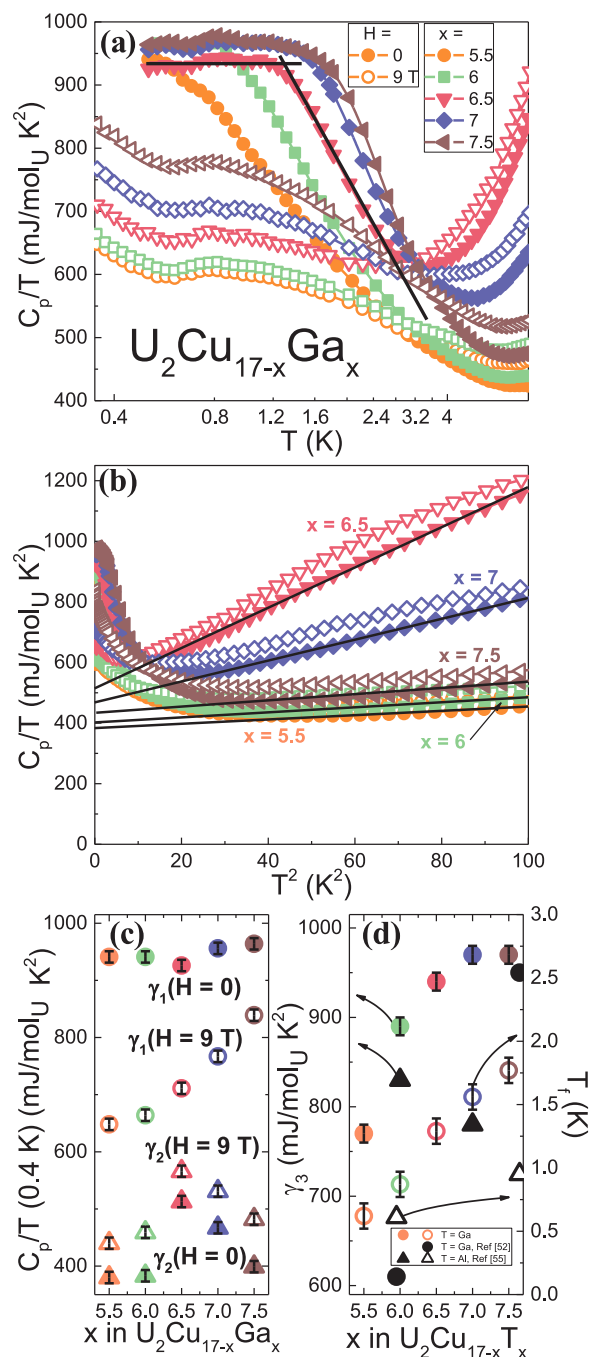


FIG. 4. Specific heat of $U_2Cu_{17-x}Ga_x$ for $5.5 \leq x \leq 7.5$. (a) Semilogarithmic plot of the specific heat C_p/T as a function of T : γ_1 values are taken as C_p/T at lowest T . Solid symbols correspond to $H = 0$ data, while open symbols represent data taken in a magnetic field $H = 9 \text{ T}$. The freezing temperature T_f is determined as the intersection of the plateau region and the region for which $C_p/T \propto \log_{10} T$, with an example shown for the $x = 6.5$ sample. (b) C_p/T as a function of T^2 , with black lines representing high-temperature fits from which the values of γ_2 are extracted. (c) Evolution of γ_1 (circles) and γ_2 (triangles) as a function of field ($H = 0$ is shown as solid symbols, while $H = 9 \text{ T}$ data are represented by open symbols). (d) γ_3 (left axis, solid symbols) and freezing temperature T_f (right axis, open symbols) as a function of x in $U_2Cu_{17-x}T_x$. $T = \text{Ga}$ data are shown by circles (black, Ref. [52]; colored, current work), while $T = \text{Al}$ data [55] are shown by triangles.

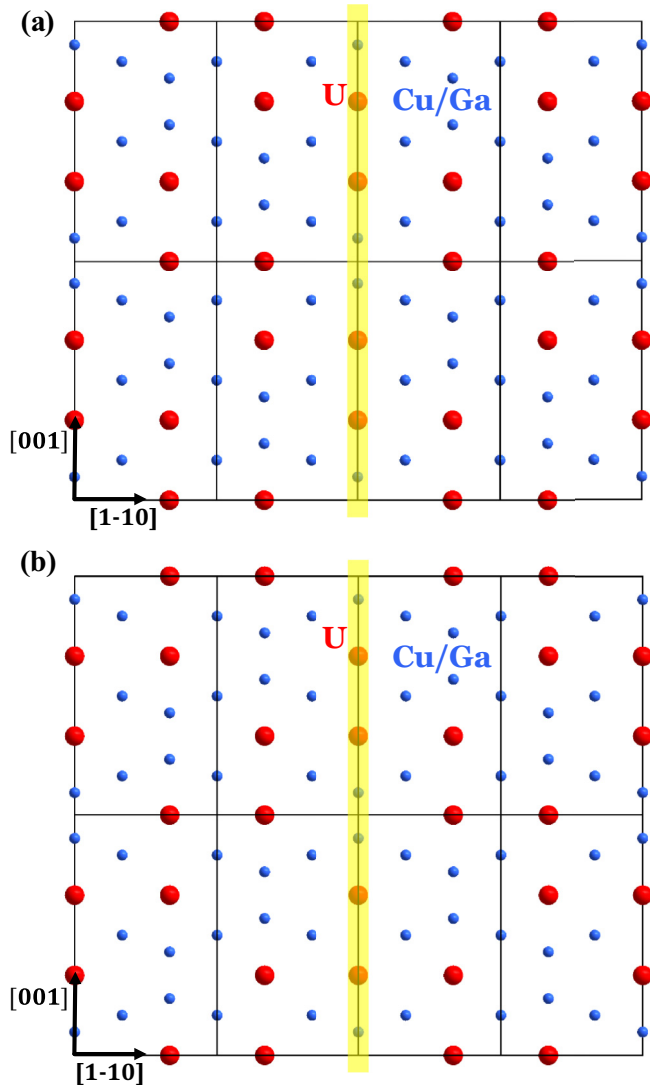


FIG. 5. Projection of a part of the local atomic arrangement in $U_2Cu_{17-x}Ga_x$ (a) without and (b) with a twin boundary present. The twin boundary is highlighted in yellow.

strength. This type of crystallographic disorder can give rise to phenomena such as enhanced effective mass and non-Fermi-liquid behavior [77–80]. Deconvoluting the role of twinning-produced disorder from that driven by Cu and Ga mixing can be achieved only if investigations regarding the presence of twinning are carried out for U_2Zn_{17} and $U_2Cu_{17-x}Al_x$ systems.

Resistivity of the $U_2Cu_{17-x}Ga_x$ ($5.5 \leq x \leq 7.5$) materials is Kondo-like, increasing ρ with decreasing T , as is evident from Fig. 6. It can be seen that the upturn in $\rho(T)$ is largest for the $x = 5.5$ sample, which has the smallest unit cell volume. This is similar to what has been reported for the case of $U_{1-x}M_xPd_2Al_3$ ($M = Y, La, \text{ and } Th$) [81]: both the La and Th substitutions resulted in an expansion of the unit cell and an upturn in $\rho(T)$ at low temperatures, while substitution with Y shows no change in volume and a drop in $\rho(T)$ at low temperatures. The overall evolution of resistivity with temperature is similar to Pd-substituted UCu_5 [82,83], Y/Th [7,15,73,76,84,85] and Sc/B-substituted [28,29] UPd_3 , Th-

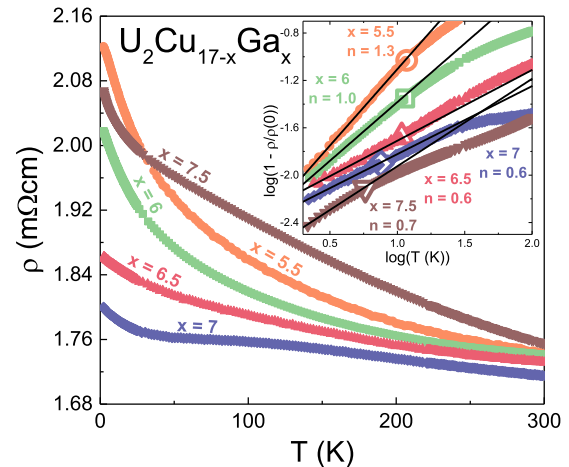


FIG. 6. Resistivity data scaled by their room-temperature value for $U_2Cu_{17-x}Ga_x$ ($5.5 \leq x \leq 7.5$). Inset: low-temperature data show linearity over more than a decade in temperature. Values of n in $1 - \rho(T)/\rho(0) = a(T/T_K)^n$ are listed for respective x . The values of T_K are marked by large symbols.

[12,86–89] and La-substituted [81] UPd_2Al_3 , and URh_2Ge_2 [33,34]. From the inset of Fig. 6, non-Fermi-liquid behavior is evident, as $1 - \rho(T)/\rho(0) = a(T/T_K)^n$, with $0.6 \leq n \leq 1.3$, which is significantly different from the conventional Kondo effect, for which $n = 2$ is expected [8]. Kondo temperatures were taken as the point at which the resistivity data deviate from the logarithmic behavior, akin to what has been done for other uranium-based systems [32,42]. The values of the Kondo temperature, $5.8 \text{ K} \leq T_K \leq 11.7 \text{ K}$, are comparable to $1/3|\theta_W|$ (Table IV), which is what has been observed for many other f -electron systems with non-Fermi-liquid behavior [6]. Gradual suppression of T_K with x is consistent with reduced mixing disorder as $x \rightarrow 8.5$, corresponding to the 50 : 50 Cu-to-Ga ratio.

The maximum value of $T_K = 11.7 \text{ K}$ is attained for the $x = 5.5$ composition, which has the smallest unit cell volume. This can be understood from the fact that the Kondo temperature T_K is proportional to the s - f exchange interaction J and the density of states at the Fermi level $N(0)$ as $T_K \propto e^{-1/JN(0)}$. The exchange interaction J , in turn, is directly proportional to the hybridization strength V_{sf} and inversely proportional to the energy difference ϵ_{5f} between the $5f$ and Fermi level [85]. Since V_{sf} increases and ϵ_{5f} decreases with decreasing volume, J is enhanced. This enhancement is larger than the decrease of the density of states at the Fermi level, caused by the increased band overlap, resulting in an overall higher T_K . A similar effect has been achieved in Y-substituted UPd_3 [85,90] with application of pressure.

IV. CONCLUSIONS

In this work, a heavy-fermion phase $U_2Cu_{17-x}Ga_x$ ($5.5 \leq x \leq 7.5$) was investigated. It was established that all materials undergo a glassy transition at $0.6 \text{ K} \leq T_f \leq 1.8 \text{ K}$. This is comparable to the $U_2Cu_{17-x}Al_x$ system, for which spin-glass behavior was observed below $1 \text{ K} < T_f < 3 \text{ K}$. Within the $U_2Cu_{17-x}Ga_x$ series, T_f increases as a function of x , which can

perhaps be explained by the increase in electron concentration as Cu atoms are substituted by Ga, which in turn enhances U-U correlations [given the itinerant nature of U atoms, an increase in $N(0)$ will likely enhance J]. On the other hand, the Kondo temperature T_K decreases as a function of x , which is likely caused by diminished disorder effects and lattice expansion, which, in turn, decreases the hybridization between the $5f$ states and the conduction electrons.

All samples of the $U_2Cu_{17-x}Ga_x$ ($5.5 \leq x \leq 7.5$) series exhibit remarkably high values of the Sommerfeld coefficient $\gamma \geq 900$ mJ/molU K². The values of γ are higher than those for U_2Zn_{17} and $U_2Cu_{17-x}Al_x$ systems, which can likely be explained by intermediate crystallographic disorder effects in the $U_2Cu_{17-x}Ga_x$ system. Within the $U_2Cu_{17-x}Ga_x$ series, the electronic specific heat coefficient γ is virtually independent of x , indicating that the role of lattice compression as well as electron concentration is likely minimal.

Moreover, a breakdown of Fermi-liquid theory is observed for all compositions, as evidenced by logarithmic divergence of magnetic susceptibility, specific heat, and electrical re-

sistivity. Typically, non-Fermi-liquid behavior is observed close to a quantum critical point, which can be induced by pressure, chemical substitution, or magnetic field. However, in dilute f -electron systems, disorder can be the source of the non-Fermi-liquid behavior, which is the case here. The $U_2Cu_{17-x}Ga_x$ materials are similar to diluted heavy-fermion systems like substituted UCu_5 , UAl_2 , UPd_3 , and UPd_2Al_3 , for which antiferromagnetism is distant in the phase diagram. The $U_2Cu_{17-x}Ga_x$ system provides a convenient way to investigate the role that disorder, electron concentration, and lattice compression play in governing the physical properties of heavy-fermion materials that exhibit non-Fermi-liquid behavior.

ACKNOWLEDGMENTS

We would like to thank M. Bobnar for NMR measurements and U. Burkhardt for assistance with SEM measurements. We are also grateful to L. Akselrud, W. Schnelle, K. Putkonen, and H. Rosner for useful discussions.

-
- [1] G. R. Stewart, *Rev. Mod. Phys.* **56**, 755 (1984).
 - [2] G. R. Stewart, *Rev. Mod. Phys.* **73**, 797 (2001).
 - [3] G. R. Stewart, *Rev. Mod. Phys.* **78**, 743 (2006).
 - [4] H. v. Löhneysen, A. Rosch, M. Vojta, and P. Wölfle, *Rev. Mod. Phys.* **79**, 1015 (2007).
 - [5] S. Wirth and F. Steglich, *Nat. Rev. Mater.* **1**, 16051 (2016).
 - [6] M. B. Maple, M. C. de Andrade, J. Herrmann, Y. Dalichaouch, D. A. Gajewski, C. L. Seaman, R. Chau, R. Movshovich, M. C. Aronson, and R. Osborn, *J. Low Temp. Phys.* **99**, 223 (1995).
 - [7] H. v. Löhneysen, *Physica B (Amsterdam, Neth.)* **206–207**, 101 (1995).
 - [8] M. B. Maple, C. L. Seaman, D. A. Gajewski, Y. Dalichaouch, V. B. Barbeta, M. C. de Andrade, H. A. Mook, H. G. Lukefahr, O. O. Bernal, and D. E. MacLaughlin, *J. Low Temp. Phys.* **95**, 225 (1994).
 - [9] B. Coqblin, *Strongly Correlated Electron Behaviors and Heavy Fermions in Anomalous Rare-Earth and Actinide Systems* (AIP, New York, 2006).
 - [10] M. B. Maple, *J. Phys. Soc. Jpn.* **74**, 222 (2005).
 - [11] M. B. Maple, R. E. Baumbach, N. P. Butch, J. J. Hamlin, and M. Janoschek, *J. Low Temp. Phys.* **161**, 4 (2010).
 - [12] P. V. Plessis, A. M. Strydom, R. Troc, T. Cichorek, C. Marucha, and R. P. Gers, *J. Phys. Condens. Matter* **11**, 9775 (1999).
 - [13] M. B. Maple, R. P. Dickey, J. Herrmann, M. C. de Andrade, E. J. Freeman, D. A. Gajewski, and R. Chau, *J. Phys. Condens. Matter* **8**, 9773 (1996).
 - [14] P. Schlottmann and P. D. Sacramento, *Adv. Phys.* **42**, 641 (1993).
 - [15] C. L. Seaman, M. B. Maple, B. W. Lee, S. Ghamaty, M. S. Torikachvili, J. S. Kang, L. Z. Liu, J. W. Allen, and D. L. Cox, *Phys. Rev. Lett.* **67**, 2882 (1991).
 - [16] B. Andraka and A. M. Tsvetlik, *Phys. Rev. Lett.* **67**, 2886 (1991).
 - [17] S. D. Wilson, P. Dai, D. T. Adroja, S. H. Lee, J. H. Chung, J. W. Lynn, N. P. Butch, and M. B. Maple, *Phys. Rev. Lett.* **94**, 056402 (2005).
 - [18] E.-W. Scheidt, T. Schreiner, K. Heuser, S. Koerner, and G. R. Stewart, *Phys. Rev. B* **58**, R10104(R) (1998).
 - [19] M. A. L. de la Torre, J. A. Gonzalez, A. Izquierdo, S. Vieira, M. Ellerby, and K. A. McEwen, *J. Appl. Phys.* **87**, 5126 (2000).
 - [20] R. Vollmer, S. Mock, T. Pietrus, H. v. Löhneysen, R. Chau, and M. B. Maple, *Physica B (Amsterdam, Neth.)* **230–232**, 603 (1997).
 - [21] F. Mayr, G. F. v. Blackenhagen, and G. R. Stewart, *Phys. Rev. B* **55**, 947 (1997).
 - [22] M. A. L. de la Torre, O. J. Dura, M. Ellerby, K. A. McEwen, and M. B. Maple, *J. Magn. Magn. Mater.* **320**, e443 (2008).
 - [23] Y. Aoki, K. Terayama, H. Sato, K. Maeda, and Y. Onuki, *Physica B (Amsterdam, Neth.)* **206–207**, 451 (1995).
 - [24] M. B. Maple, D. A. Gajewski, R. Chau, H. A. Mook, R. Movshovich, and C. L. Seaman, *Physica B (Amsterdam, Neth.)* **223–224**, 447 (1996).
 - [25] C. L. Seaman and M. B. Maple, *Physica B (Amsterdam, Neth.)* **199–200**, 396 (1994).
 - [26] M. A. López de la Torre, J. Rodríguez Fernández, and K. A. McEwen, *J. Appl. Phys.* **79**, 6364 (1996).
 - [27] M. A. L. de la Torre, J. R. Fernández, K. A. McEwen, and M. B. Maple, *Phys. Rev. B* **74**, 014431 (2006).
 - [28] S. K. Dhar, K. Ghosh, and S. Ramakrishnan, *Physica B (Amsterdam, Neth.)* **223–224**, 215 (1996).
 - [29] D. A. Gajewski, R. Chau, and M. B. Maple, *Phys. Rev. B* **62**, 5496 (2000).
 - [30] R. P. Dickey, E. J. Freeman, V. S. Zapf, P. C. Ho, and M. B. Maple, *Phys. Rev. B* **68**, 144402 (2003).
 - [31] D. P. Rojas, L. M. da Silva, A. N. Medina, F. G. Gandra, L. P. Cardoso, and J. C. Waerenborgh, *J. Magn. Magn. Mater.* **272–276**, E1 (2004).
 - [32] V. S. Zapf, R. P. Dickey, E. J. Freeman, C. Sirvent, and M. B. Maple, *Phys. Rev. B* **65**, 024437 (2001).
 - [33] S. Süllow, S. A. M. Mentink, T. E. Mason, R. Feyerherm, G. J. Nieuwenhuys, A. A. Menovsky, and J. A. Mydosh, *Phys. Rev. B* **61**, 8878 (2000).

- [34] S. Sullow, I. Maksimov, A. Otop, F. J. Litterst, A. Perucchi, L. Degiorgi, and J. A. Mydosh, *Phys. Rev. Lett.* **93**, 266602 (2004).
- [35] E. Miranda, V. Dobrosavljevic, and G. Kotliar, *Phys. Rev. Lett.* **78**, 290 (1997).
- [36] E. Miranda, V. Dobrosavljevic, and G. Kotliar, *J. Phys. Condens. Matter* **8**, 9871 (1996).
- [37] E. Miranda and V. Dobrosavljevic, *Rep. Prog. Phys.* **68**, 2337 (2005).
- [38] B. Coqblin, *Acta Phys. Pol.* **118**, 913 (2010).
- [39] A. H. Castro Neto, G. Castilla, and B. A. Jones, *Phys. Rev. Lett.* **81**, 3531 (1998).
- [40] A. H. Castro Neto and B. A. Jones, *Phys. Rev. B* **62**, 14975 (2000).
- [41] S. Yotsuhashi, K. Miyake, and H. Kusunose, *J. Phys. Soc. Jpn.* **71**, 389 (2002).
- [42] V. H. Tran, *Acta Phys. Pol. A* **113**, 387 (2008).
- [43] A. Misiuk, J. Mulak, and A. Czopnik, *Bull. Acad. Pol. Sci.* **21**, 487 (1973).
- [44] H. E. Fischer, E. T. Swartz, R. O. Pohl, B. A. Jones, J. W. Wilkins, and Z. Fisk, *Phys. Rev. B* **36**, 5330 (1987).
- [45] H. R. Ott, H. Rudigier, Z. Fisk, and J. L. Smith, *Phys. Rev. Lett.* **50**, 1595 (1983).
- [46] V. A. Sidorov, J. D. Thompson, and Z. Fisk, *J. Phys. Condens. Matter* **22**, 406002 (2010).
- [47] J. O. Willis, Z. Fisk, and G. R. Stewart, *J. Magn. Magn. Mater.* **54–57**, 395 (1986).
- [48] M. Olivier, T. Siegrist, and S. P. McAlister, *Phys. Rev. B* **35**, 5025 (1987).
- [49] G. F. von Blanckenhagen, E. W. Scheidt, T. Schreiner, and G. R. Stewart, *Phys. Rev. B* **64**, 064413 (2001).
- [50] J. Stepien-Damm, V. H. Tran, L. Shlyk, and R. Troc, *J. Alloys Compd.* **205**, 291 (1994).
- [51] Y. Verbovysky and A. P. Goncalves, *Intermetallics* **33**, 16 (2013).
- [52] R. Troc, B. Andraka, M. Kuznietz, V. H. Tran, A. M. Gurevich, M. Wolczyk, and D. Badurski, *Physica B (Amsterdam, Neth.)* **230–232**, 65 (1997).
- [53] T. Nishioka, K. Mizutani, S. Taniguchi, and M. Kontani, *J. Magn. Magn. Mater.* **177–181**, 451 (1998).
- [54] Y. Oohara, M. Kubota, H. Yoshizawa, S. Itoh, T. Nishioka, and M. Kontani, *J. Phys. Chem. Solids* **60**, 1197 (1999).
- [55] R. Pietri, B. Andraka, R. Troc, and V. H. Tran, *Phys. Rev. B* **56**, 14505 (1997).
- [56] G. Cordier, E. Czech, H. Schafer, and P. Woll, *J. Less Common. Met.* **110**, 327 (1985).
- [57] A. Leithe-Jasper, H. Borrmann, and W. Hönl, Max-Planck-Institut für Chemische Physik fester Stoffe Scientific Report, 2003–2005 (2006), pp. 24–27.
- [58] STOE Powder Software, WINXPOW, version 2, STOE and Cie GmbH, Darmstadt, Germany, 2001.
- [59] L. Akselrud and Y. Grin, *J. Appl. Crystallogr.* **47**, 803 (2014).
- [60] T. Siegrist and Y. L. Page, *J. Less Common. Met.* **127**, 189 (1987).
- [61] R. Herbs-Irmer and G. M. Sheldrick, *Acta Crystallogr., Sect. B* **58**, 477 (2002).
- [62] K. P. Hilleke, R. T. Fredrickson, A. I. Vinokur, and D. C. Fredrickson, *Cryst. Growth Des.* **17**, 1610 (2017).
- [63] S. Ikeda, S. Nishigori, T. Suzuki, T. Fujita, Y. Maeda, T. Takabatake, and H. Fujii, *Physica B (Amsterdam, Neth.)* **194–196**, 465 (1994).
- [64] D. Kaczorowski, P. W. Klamut, A. Czopnik, and A. Jeżowski, *J. Magn. Magn. Mater.* **177–181**, 41 (1998).
- [65] M. H. V. Maaren, H. J. V. Daal, K. H. J. Buschow, and C. J. Schinkel, *Solid State Commun.* **14**, 145 (1974).
- [66] K. H. J. Buschow, *J. Less Common. Met.* **31**, 165 (1973).
- [67] E. Svanidze, A. Amon, A. Leithe-Jasper, and Y. Grin (2018).
- [68] M. Samsel-Czekafa, E. Talik, P. de V. Du Plessis, R. Troc, H. Misiorek, and C. Sulkowski, *Phys. Rev. B* **76**, 144426 (2007).
- [69] J. F. Counsell, R. M. Dell, and J. F. Martin, *Trans. Faraday Soc.* **62**, 1736 (1965).
- [70] H. Hill, *Plutonium 1970 and Other Actinides* (AIME, New York, 1970).
- [71] J. A. Mydosh, *Spin Glasses: An Experimental Introduction* (Taylor and Francis, London, 1993).
- [72] K. Binder and A. P. Young, *Rev. Mod. Phys.* **58**, 801 (1986).
- [73] H. G. Lukefahr, O. O. Bernal, D. E. MacLaughlin, C. L. Seaman, M. B. Maple, and B. Andraka, *Phys. Rev. B* **52**, 3038 (1995).
- [74] A. Otop, S. Sullow, E. W. Scheidt, and J. A. Mydosh, *Phys. Rev. B* **77**, 045121 (2008).
- [75] H. Walker, K. McEwen, E. Colineau, J. C. Griveau, and F. Wastin, *J. Magn. Magn. Mater.* **310**, 751 (2007).
- [76] C. L. Seaman, M. B. Maple, B. W. Lee, S. Ghamaty, M. S. Torikachvili, J. S. Kang, L. Z. Liu, J. W. Allen, and D. L. Cox, *J. Alloys Compd.* **181**, 327 (1992).
- [77] A. N. Christensen and R. G. Hazell, *Acta Chem. Scand., Ser. A* **34a**, 455 (1980).
- [78] S. Cirafici and A. Palenzona, *Thermochim. Acta* **162**, 117 (1990).
- [79] V. Levytskyy, A. Kostetzka, V. Babizhekkii, B. Kotur, and R. Serkiz, *Visn. L'viv. Derzh. Univ., Ser. Khim.* **54**, 19 (2013).
- [80] R. Lemaire and D. Paccard, *Bull. Soc. Fr. Mineral. Cristallogr.* **92**, 9 (1969).
- [81] V. S. Zapf, E. J. Freeman, R. P. Dickey, P. C. Ho, and M. B. Maple, *Physica B (Amsterdam, Neth.)* **312–313**, 448 (2002).
- [82] A. Weber, S. Korner, E. W. Scheidt, S. Kehrein, and G. R. Stewart, *Phys. Rev. B* **63**, 205116 (2001).
- [83] B. Andraka and G. R. Stewart, *Phys. Rev. B* **47**, 3208 (1993).
- [84] A. M. Strydom and P. de V. Du Plessis, *Acta Phys. Pol.* **98**, 593 (2000).
- [85] G. Oomi, T. Kagayama, Y. Aoki, H. Sato, Y. Onuki, H. Takahashi, and N. Mori, *J. Phys. Condens. Matter* **16**, 3385 (2004).
- [86] Y. Dalichaouch and M. B. Maple, *Physica B: Condensed Matter* **199–200**, 176 (1994).
- [87] R. P. Dickey, A. Amann, E. J. Freeman, M. C. de Andrade, and M. B. Maple, *Phys. Rev. B* **62**, 3979 (2000).
- [88] M. B. Maple, A. Amann, R. P. Dickey, E. J. Freeman, C. Sirvent, M. C. de Andrade, and N. R. Dilley, *Physica B (Amsterdam, Neth.)* **281–282**, 332 (2000).
- [89] P. de V. du Plessis, A. M. Strydom, and R. P. Gers, *Physica B (Amsterdam, Neth.)* **230–232**, 610 (1997).
- [90] Y. Sakurai, T. Kagayama, G. Oomi, Y. Aoki, H. Sato, Y. Onuki, H. Takahashi, and N. Mori, *Physica B (Amsterdam, Neth.)* **230–132**, 596 (1997).